
# Dynamic in situ imaging of semi-hard cheese microstructure under large-strain tensile deformation: Understanding structure-fracture relationships

Prabin Lamichhane, Mark A.E. Auty, Alan L. Kelly, Jeremiah J. Sheehan

PII: S0958-6946(19)30263-8

DOI: https://doi.org/10.1016/j.idairyj.2019.104626

Reference: INDA 104626

To appear in: *International Dairy Journal*

Received Date: 15 August 2019

Revised Date: 4 December 2019

Accepted Date: 5 December 2019

Please cite this article as: Lamichhane, P., Auty, M.A.E., Kelly, A.L., Sheehan, J.J., Dynamic in situ imaging of semi-hard cheese microstructure under large-strain tensile deformation: Understanding structure-fracture relationships, *International Dairy Journal*, https://doi.org/10.1016/j.idairyj.2019.104626.

# Dynamic in situ imaging of semi-hard cheese microstructure under large-strain tensile deformation: Understanding structure-fracture relationships

Prabin Lamichhane[a,b], Mark A. E. Auty[a,1], Alan L. Kelly[b], Jeremiah J. Sheehan[a]*

[a] *Teagasc Food Research Centre, Moorepark, Fermoy, Co. Cork, Ireland P61 C996*

[b] *School of Food and Nutritional Sciences, University College Cork, Ireland T12 YN60*

* Corresponding author. Tel.:

*E-mail address*: diarmuid.sheehan@teagasc.ie (J. J. Sheehan)

[1] Present address:

Mondelez International Ltd., Reading Science Centre, Whiteknights Campus, Reading, RG6 6LA, UK

ABSTRACT

Changes in the microstructure of semi-hard cheeses were observed in situ under tensile deformation by placing a microtensile stage directly under a confocal scanning laser microscope, and recording force/displacement data simultaneously. On tensile deformation, detachment of fat globules and their subsequent release from the cheese matrix were observed, suggesting that they are weakly bonded to or entrapped within the cheese matrix. Moreover, an inherent micro-defect was observed at a curd granule junction within the cheese matrix, which fractured along the curd granule junction under tensile deformation, suggesting that such micro-defects could be a key to the formation of undesirable slits or cracks. Furthermore, the fracture behaviour of semi-hard cheese varied with ripening temperature, coagulant type, and inhibition of residual chymosin activity. Overall, this study demonstrated the potential of dynamic in situ imaging of cheese microstructure for developing a greater understanding of the breakdown behaviour of cheese matrices.

## 1. Introduction

Food matrices go through a series of structure formation (e.g., gel formation) and breakdown (e.g., during mastication) processes during manufacture, storage and consumption. Understanding these processes from a structural point of view is of growing interest to researchers and food producers, as many of the desirable properties/functionalities of foods are determined by their structure (Lamichhane, Kelly, & Sheehan, 2018a).

To date, considerable success has been achieved in visualisation of food microstructure at multiple scales by utilising various microscopy techniques (El-Bakry & Sheehan, 2014; Everett & Auty, 2008, 2017; Ong, Dagastine, Kentish, & Gras, 2011). Several studies have shown the potential of dynamic in situ imaging of food microstructure for comprehensive understanding of the physical changes to food structure when subjected to various conditions relevant to processing, storage or consumption, such as heating/cooling, shearing, compression and tension. For example, Auty, Fenelon, Guinee, Mullins, and Mulvihill (1999) studied the milk gelation and cheese melting process using a hot-stage placed under a confocal scanning laser microscopy (CSLM) instrument. Other studies investigated the structural and mechanical changes under large-strain deformation of gels, e.g., whey protein isolate gels, emulsion filled gels, and stirred acid milk gels (Abhyankar, Mulvihill, & Auty, 2011, 2014; Brink, Langton, Stading, & Hermansson, 2007) and meat (James & Yang, 2011) using a microtensile stage coupled with CSLM or environmental scanning electron microscopy (ESEM). Boitte, Hayert, and Michon (2013) visualised the microstructure of dough under shear (relevant to dough processing condition) using a rheo-optical device. Liu, Stieger, van der Linden, and van de Velde (2015) observed the microstructure of gels under shear to better understand the role of fat droplet characteristics on fat-related sensory perception. Geng, van den Berg, Bager, and Ipsen (2011) developed a

setup for dynamic visualisation of syneresis of cheese curd during mechanical treatment. Somaratne et al. (2020) investigated the real-time disintegration behaviours of egg white protein gels using an in situ gastric digestion methodology based on high-resolution time-lapse confocal microscopy. Similarly, Zhang, Jung, Zhang, Muriel Mundo, and McClements (2019) monitored in situ lipid droplet release patterns from biopolymer microgels under simulated gastric conditions using magnetic resonance imaging and spectroscopy.

Although a number of studies have monitored the structure of model food systems or complete foods, there are no published data on the physical changes to the structure of cheese under large-strain deformation. Cheese is an inhomogeneous composite material, in which individual curd granules bind together, and where granule junctions remain between individual curd granules. Visualisation of cheese microstructure under large-strain deformation may help to understand sensory perception, flavour and nutrient release, and the mechanisms of formation of undesirable slits and cracks within the cheese matrix.

From a materials science perspective, cheese can be viewed as a two-phase composite material containing fat globules as a filler in a protein gel matrix (Barden, Osborne, McMahon, & Foegeding, 2015; Lamichhane et al., 2018a). Studies have shown that the sensory perception of food is influenced by filler-matrix interactions; e.g., emulsion-filled gels with unbound fat droplets exhibit stronger fat-related sensory perceptions than bound fat droplets (Liu et al., 2015; Sala, van de Velde, Cohen Stuart, & van Aken, 2007). Visualisation of cheese microstructure under large-strain deformation may help to understand fat-protein interaction within the cheese matrix. Moreover, dynamic in situ imaging may help to identify weak spots within the cheese matrix which are seeds for the development of slits/cracks within the cheese matrix. Development of undesirable slits and cracks is a major problem in the manufacture of Swiss, Dutch and related eye-type cheeses, leading to

downgrading of the product and lost revenue to manufacturers (Guggisberg et al., 2015; White, Broadbent, Oberg, & McMahon, 2003).

The breakdown properties of cheese depends on composition, manufacturing procedures, maturation profile, environmental conditions (e.g., pH, temperature, and solvent quality/ionic strength), and the presence of defects (such as mechanical holes, slits and cracks), among other factors (Luyten, 1988; Visser, 1991). Extensive hydrolysis of $\alpha_{S1}$-casein has been reported in some semi-hard eye-type cheeses (McGoldrick & Fox, 1999), especially during the warm-room ripening stage, mainly due to residual chymosin activity. Intact $\alpha_{S1}$-casein is considered important for maintaining the elastic texture of eye-type cheeses, which is vital to accommodate gas produced by microorganisms (Daly, McSweeney, & Sheehan, 2010). Previous studies have shown that the substitution of fermentation-produced bovine chymosin (FPBC) with fermentation-produced camel chymosin (FPCC) reduced the primary hydrolysis of $\alpha_{S1}$-casein during ripening in different cheese types (Bansal et al., 2009; Soodam, Ong, Powell, Kentish, & Gras, 2015).

Although previous studies have investigated the influence of factors, such as maturation, chymosin-mediated proteolysis, ripening temperature and coagulant types, on texture and fracture properties of different cheese varieties (Lamichhane, Sharma, Kennedy, Kelly, & Sheehan, 2019; McCarthy, Wilkinson, & Guinee, 2017; O'Mahony, Lucey, & McSweeney, 2005; Soodam et al., 2015), there is limited understanding on the influence of such factors on changes to the microstructure of cheese under large-strain deformation. The primary objective of this study was to achieve dynamic in situ imaging of cheese microstructure under tensile deformation. The secondary objective of this study was to investigate the effect of maturation, ripening temperature, coagulant type and chymosin-mediated proteolysis on changes in microstructure and fracture behaviour of cheeses under tensile deformation, using a microtensile stage and CSLM. The current study was undertaken

as an element of a larger study to differentiate the effects of primary proteolysis and calcium solubilisation on the fracture properties of semi-hard cheese (Lamichhane et al., 2019). Levels of primary proteolysis, pH, breakdown patterns of caseins, and insoluble calcium contents of the cheeses analysed in the current study were reported by Lamichhane et al. (2019).

## 2. Materials and methods

### *2.1. Cheese manufacture*

Four variants of a washed-curd, brine-salted semi-hard cheese, i.e., control cheese, cheese without warm-room ripening (noWR), cheese made using FPCC as a coagulant (CC), and cheese containing a chymosin inhibitor, i.e., pepstatin A, which was added to the curd/whey mixture during cheese manufacture (PepA), were manufactured in three replicate trials as reported in Lamichhane et al. (2019). Briefly, all cheese milk samples used in this study were standardised (protein to fat ratio of 1.1: 1.0) and pasteurised (72 °C for 15 s). Frozen direct vat inoculation cultures (Chr. Hansen Ltd., Cork, Ireland) were used as a starter cultures: (i) R-604 (180 mg $kg^{-1}$ milk), containing *Lactococcus lactis* ssp. *cremoris* and *Lactococcus lactis* ssp. *lactis* and (ii) LH-B02 (9 mg $kg^{-1}$ milk), containing *Lactobacillus helveticus*. For control, noWR and PepA cheeses, FPBC (CHY-MAX Plus, ~200 international milk clotting units (IMCU) $mL^{-1}$; Chr. Hansen Ltd., Cork, Ireland) was added at a level of 0.18 mL $kg^{-1}$ cheese milk, whereas FPCC (CHY-MAX M, ~200 IMCU $mL^{-1}$; Chr. Hansen Ltd.) was added at a level of 0.14 mL $kg^{-1}$ cheese milk for CC cheeses. Curd granules were washed by removing 35% of whey with subsequent addition of 23% warm (50 °C) reverse-osmosis water as a percentage of the total milk weight. Curd washing was performed

to control the pH of the cheeses after manufacture by adjustment of the residual curd lactose content. Chymosin inhibitor, i.e., pepstatin A, was added at a rate of 10.0 μmol $kg^{-1}$ cheese milk into the curd/whey mixture for PepA cheese manufacture. Whey was drained when the curd pH reached 6.35, and the curds were collected into moulds and pressed vertically. After pressing, each cheese wheel (600 g) was placed in a saturated brine solution for 7.5 h at 8 °C prior to vacuum packaging (Falcon 52, Original Henkelman vacuum system, the Netherlands). A summary of the experimental plan, including ripening regimens, is shown in Supplementary material Table S1.

### *2.2. Cheese composition*

Grated cheese samples were analysed in duplicate for content of moisture, fat, protein, salt, and total calcium and for pH as reported in Lamichhane et al. (2019).

### *2.3. Tensile testing and in situ imaging of cheese microstructure*

A schematic of the experimental set-up for tensile testing is shown in Fig. 1. Cylindrical samples of diameter 30 mm were removed from each experimental cheese using a stainless-steel borer. From each cylindrical sample, thin cheese discs (thickness ~4 mm and diameter 30 mm) were prepared using a 4-mm thick plastic ring and sharp scalpel. Cheese samples of dimensions 25 mm × 10 mm × 4 mm were removed from these thin cheese discs, and a small indentation (~1.5 mm), also called a notch, was made in the centre of each test piece using a sharp scalpel. The exact thickness of samples was determined afterwards using a Vernier calliper. The mean thickness of eight representative samples was 4.09 mm, with a standard deviation of 0.33 mm. The test samples were then clamped between the grips of a

163 micro-tensile stage (Deben, UK), equipped with 2 N load cell and motorised gear box. The
164 gap between the clamps was 10 mm.

165 Fast Green (protein specific dye; Sigma Aldrich, Cork, Ireland) and Nile Red (fat
166 specific dye; Sigma Aldrich) of concentration 0.01% (w/v), prepared in deionised water and
167 in 1,2-propanediol respectively, were mixed in a ratio of 1:3 (Le Tohic et al., 2018). The
168 prepared dye (10 μL) was poured on the cheese samples and a cover slip (diameter = 9 mm,
169 VWR International Limited, Dublin, Ireland) was gently placed on the clamped test samples
170 to avoid the entrapment of air bubbles. The micro-tensile stage was placed directly under the
171 CSLM (Leica Microsystems). Five minutes after dye addition, the test samples were
172 elongated at a constant tensile speed of 2 mm $min^{-1}$ and images of cheese microstructure were
173 simultaneously taken using air objectives of magnification of 5× or 10× (zoom factor 2 or 3).
174 Protein and fat phases in the cheese samples were visualised by exciting the Fast Green
175 (using a helium-neon laser) and Nile Red (using an Argon laser) dyes, respectively, as
176 described by Abhyankar et al. (2014). Load and displacement data of the test samples were
177 recorded every 500 ms, which were then converted to true stress ($\sigma$; Equation 1) and Hencky
178 strain ($\varepsilon_H$; Equation 2) (Abhyankar et al., 2011):

179 $$\sigma = \frac{F \times (L_0 + \Delta L)}{A \times L_0} \quad (1)$$

180 $$\varepsilon_H = \ln\left(\frac{L_0 + \Delta L}{L_0}\right) \quad (2)$$

181 where F is the extensional force, A is original cross sectional area of the sample, $L_0$ is
182 original length of the sample and ΔL is change in length of sample.

183 The crack length of test samples during tensile deformation was measured as
184 described by Abhyankar et al. (2011), using the Leica Application Suit X software (Leica
185 Microsystems, Baden-Württemberg, Germany). Crack length was defined as the

perpendicular distance between the tip of an artificial notch (at time zero) and the tip of the new fracture surface (at time t) during tensile deformation. Young's modulus was calculated from the slope of the initial linear region of stress-strain curve (Bast et al., 2015). Fracture stress and fracture strain values of cheese samples were determined from the inflection point of the stress-strain curve. At least four samples, from two independent replicate trials, of each cheese were tested on the microtensile unit to determine the effect of maturation and treatment on the structural breakdown behaviour of experimental cheeses. All measurements were conducted at room temperature (~20 °C).

### *2.4. Statistical analysis*

Statistical analyses of the data were performed using SigmaPlot version 14 (Systat Software, Inc., San Jose, CA, USA). The effect of maturation and treatment on cheese fracture parameters was determined performing one way ANOVA followed by post hoc Tukey tests (Granato, de Araújo Calado, & Jarvis, 2014). Before ANOVA evaluation, data were checked for normality and homoschedasticity by performing Shapiro–Wilk and Brown–Forsythe tests, respectively. When these assumptions were not verified, appropriate non-parametric and post hoc tests were applied (Granato et al., 2014). The level of significance was set at $P \leq 0.05$.

## 3. Results and discussion

### *3.1. Cheese composition*

The compositional parameters of the cheeses analysed here were described in detail by Lamichhane et al. (2019) and in Supplementary material Table S2. The cheeses had a composition typical of that of Maasdam-type cheese (Lamichhane, Kelly, & Sheehan, 2018b; Lamichhane et al., 2018c; Panthi et al., 2019). Treatment had no significant effect ($P < 0.05$) on mean levels of moisture, moisture-in non-fat substance, protein, fat, fat-in-dry matter, salt, salt-in-moisture, total calcium and pH (at 1 d of ripening) of the cheeses.

### *3.2. Effect of maturation on structural breakdown behaviour of cheese*

To determine the effect of maturation on structural breakdown behaviour of cheese, control cheese samples at 20 d (before warm-room ripening), 48 d (after warm-room ripening) and 90 d of ripening were tested on the microtensile unit.

Representative stress-strain relationships of control cheese samples after 20 d, 48 d and 90 d of ripening are shown in Fig. 2a. The stress-strain relationships of cheese samples before warm-room ripening (20 d) were found to be different compared with those of cheese samples after warm-room ripening (48 d and 90 d) (Fig. 2a). A number of parameters can be determined from the stress-strain curve, such as Young's modulus, fracture stress and fracture strain. Young's modulus measures the stiffness of the material; a higher value of Young's modulus corresponds to a higher material stiffness (Vandenberghe, Choucharina, De Ketelaere, De Baerdemaeker, & Claes, 2014). Fracture stress measures the rigidity of the material whereas the fracture strain measures the brittleness or shortness of the material (Lamichhane et al., 2019; Sharma, Munro, Dessev, Wiles, & Foegeding, 2018). Young's modulus (Fig 2b), fracture stress and fracture strain (Fig. 2c) values were significantly higher ($P < 0.05$) for cheeses before warm-room ripening than after warm-room ripening.

Changes to the microstructure of cheeses before warm-room ripening (20 d) and after warm-room ripening (48 d) were similar under tensile deformation (micrographs not shown), i.e., widening of the notch, stretching of the protein network near the leading point of notch and propagation of notch. However, the stress profile during notch propagation was different between cheeses before warm-room ripening and after warm-room ripening, which can be visualised by plotting stress versus crack length (a perpendicular distance between the tip of an artificial notch and the tip of the new fracture surface during tensile deformation as measured from the CSLM time-series micrographs). Such an approach has previously been applied to study the breakdown behaviour of different kinds of gels, such as whey protein, mixed biopolymer or emulsion-filled gels (Abhyankar et al., 2011; Brink et al., 2007; Öhgren, Langton, & Hermansson, 2004).

Representative profiles of stress versus crack length for cheese samples at 20 d, 48 d and 90 d of ripening are shown in Fig. 2d; similar trends were observed in all replicate trials. For cheese samples at 48 d or 90 d of ripening, true stress increased gradually until the cheese sample started to fracture from the notch tip (Fig. 2d). Once the cheese started to fracture from the notch tip, the stress required to further break down cheese samples remained constant (Fig. 2d). However, the stress required to break down cheese at 20 d of ripening continued to increase even after the cheese sample started to fracture from the leading point of the notch; stress continued to rise until the crack length of cheese reached ~4 mm (Fig. 2d). This suggests that, as expected, the young semi-hard cheeses can resist fracture to a greater extent compared with mature cheeses.

Overall, semi-hard cheese structure becomes weak, brittle and less stiff (as indicated by lower fracture stress, fracture strain and Young's modulus values) during maturation, especially during warm-room (23 °C) ripening, which is attributed to age-related structural changes on the cheese matrix, such as proteolysis and partial solubilisation of colloidal

calcium (O'Mahony et al., 2005). During ripening, intact caseins (which are responsible for network formation) are hydrolysed by proteolytic enzymes into small and medium-sized peptides. Moreover, the calcium associated with the casein (which enhances the cross-linking of casein within the cheese matrix) solubilises partially during ripening (O'Mahony et al., 2005). The level of insoluble calcium of the cheeses of the current study decreased significantly whereas the level of primary proteolysis increased, especially during warm-room ripening (Lamichhane et al., 2019).

### *3.3. Effect of treatment on structural breakdown behaviour of cheese*

The effect of three different treatments, i.e., (i) warm-room ripening, (ii) chymosin-mediated proteolysis, and (iii) coagulant type, on structural breakdown behaviour of the semi-hard cheeses at 48 d of ripening was studied. Typical true stress and Hencky strain relationships for each experimental cheese types are shown in Fig. 3a. The CC, noWR and PepA cheeses showed similar stress-strain relationships. However, the stress-strain relationships for control cheeses were different from the other cheeses. Moreover, the fracture parameters obtained from the stress-strain curve was found to be significantly different between experimental cheese variants; Young's modulus (Fig. 3b) and fracture stress (Fig. 3c) values of CC, noWR and PepA cheeses were significantly ($P < 0.05$) higher than the control cheese at 48 d of ripening. No significant effect of treatment on fracture strain value was observed, although noWR cheeses expected to have significantly higher fracture strain value as compared with other experimental cheese type (Lamichhane et al., 2019).

Although changes to the microstructure of experimental cheeses variants at 48 d of ripening were observed to be similar under tensile deformation (micrographs not shown), stress profile as a function of crack length was found to be different between these cheeses

(Fig. 3d). Stress increased until the control cheese sample started to fracture from the notch tip during tensile deformation, followed by a levelling off in the stress with further increases in the crack length (Fig. 3d).

However, for CC, noWR and PepA cheeses, the stress required for breakdown of cheese samples continued to increase until the crack length reached ~2 mm (Fig. 3d). Fracture may occur once the stress exceeds the cohesive strength of the material (Foegeding et al., 2011). This suggests that the cohesive strength of the CC, noWR and PepA cheeses is higher as compared with the control cheeses. The different fracture behaviour of the control cheeses compared with the noWR cheeses is attributed to temperature-induced biochemical changes, mainly proteolysis, in the cheese matrix (Soodam, Ong, Powell, Kentish, & Gras, 2017), as noWR cheeses were not subjected to warm-room ripening.

The different fracture behaviour of the control and CC cheeses at 48 d of ripening was attributed to the different proteolytic activities of residual coagulants; FPBC was used as a coagulant in control cheeses, whereas in CC cheeses FPCC was used. Studies have reported that the proteolytic activity of FPCC was much lower as compared with FPBC (Kappeler et al., 2006). The extent of primary proteolysis has been found to be lower in different cheese types made with FPCC than in cheeses made with FPBC, such as Cheddar (Bansal et al., 2009; McCarthy et al., 2017), Mozzarella (Moynihan et al., 2014), and Italian soft cheese (Alinovi et al., 2018). In the current study, substitution of FPBC with FPCC as coagulant reduced the primary proteolysis of cheese during ripening (Lamichhane et al., 2019).

The different fracture behaviour of PepA cheeses as compared with control cheeses is attributed to the inhibition of residual chymosin activity (O'Mahony et al., 2005; Shakeel-Ur-Rehman, Feeney, McSweeney, & Fox, 1998) in the former cheeses where a chymosin inhibitor, i.e., pepstatin A, was added to the curd/whey mixture. This suggests that the

activity of residual chymosin may have an important influence on the fracture behaviour of semi-hard cheese.

### *3.4. Dynamic visualisation of cheese microstructures under tensile deformation*

Changes to the microstructures of cheese during tensile deformation were obtained using CSLM. Widening of the notch (Fig. 4a), stretching of the protein network (in the direction of tensile force) near the notch tip (Fig. 4b,c) and initiation of fracture from the leading point of notch (Fig. 4d) were all observed prior to propagation (i.e., rapid growth of fracture surface) of a notch (Fig. 4e,f) during tensile deformation (Supplementary material Time-lapse video 1), in all experimental cheeses, regardless of maturation level or applied treatment. Stretching of the protein network near the notch tip is due to stress concentration (Luyten, 1988).

Moreover, on tensile deformation, both small (5–7 μm) and large (15 μm) fat globules/pools (Fig. 4c, inset) near the notch tip appeared disconnected from the stretched protein networks (Fig. 4c), suggesting that the fat globules/pools within the semi-hard cheese matrix were unbound to the protein matrix or weakly held (entrapped) within the protein matrix. Furthermore, fracture propagated through protein network in all cheeses leaving fat globules/pools intact. Abhyankar et al. (2014) also reported a similar observation in a particulate gel, i.e., whey-protein-emulsion-filled gels prepared at pH 5.4. If the fat globules were attached to the protein matrix, the fracture would be more likely to propagate through the fat globules as well (Abhyankar et al., 2014).

Selected CSLM micrographs taken during tensile deformation of cheese samples are shown in Fig. 5. The time-series micrographs and Supplementary material Time-lapse video 2 clearly show release of fat from the cheese matrix. The fat pool within the circle (Fig. 5a–c)

is the same fat pool observed at different time points during tensile deformation. Utilising image analysis, the diameter of the fat pool within the circle (Fig. 5a), was found to be ~20 µm, which is higher than the average diameter of native milk fat globules i.e., 4 µm (Lopez, 2005), suggesting that the fat pool is either coalesced fat (resulting from fusion of individual fat globules) or non-globular fat (Lopez, Camier, & Gassi, 2007). Cheese manufacture steps, such as cooking and pressing, can cause aggregation, coalescence and disruption of fat globules, with the formation of non-globular fat or free fat (Lopez et al., 2007). Release of fat from the protein matrix was not only observed at the initial stages of notch propagation but was also observed at the advanced stages of notch propagation. Furthermore, the release of fat from the cheese matrix was observed at all stages of ripening (micrographs not shown). These results suggest that the applied technique is suitable for understanding fat-protein interactions within semi-hard cheese matrix.

From a materials science perspective, cheese can be viewed as a 2-phase composite material containing fat globules as a filler in a protein gel matrix (Barden et al., 2015; Lamichhane et al., 2018a). The sensory perception of foods is largely determined by properties of the filler, the extent of filler-matrix interactions, distribution of the filler, and characteristics of the gel matrix (Lamichhane et al., 2018a). A better understanding of interactions between the protein matrix and fat globules is desirable to understand the release patterns of fat globules in the mouth during mastication, which in turn will influence texture and potentially flavour perception. Studies have shown that emulsion-filled gels with unbound fat droplets exhibit stronger fat-related sensory perceptions than bound fat droplets (Liu et al., 2015; Sala et al., 2007).

To better understand the fracture behaviour at a macroscopic level, changes in cheese structure were also observed at low magnification during tensile deformation. The fracture initiated from the leading point of notch and then propagated in an irregular zig-zag manner,

probably due to the inhomogeneous nature of the cheese matrix. Similar fracture behaviour has previously been reported in whey-protein-emulsion-filled gels prepared at pH 5.4 (Abhyankar et al., 2014) and β-lactoglobulin gel (Öhgren et al., 2004). Although very little has been published regarding fracture behaviour of food materials, inhomogeneous protein-based food materials, such as meat, are likely to show a similar irregular fracture behaviour (James & Yang, 2011).

It is possible to observe, in real time, whether the fracture goes through individual curd granule or along curd granule junctions by observing cheese microstructure at low magnification. The density of the protein network at the curd granule junction (Fig. 6, short arrow) is higher compared with the interior of curd granules, due to leaching of the fat from the curd granule surface to whey during cheese manufacture. Selected CSLM micrographs (Fig. 6) taken during tensile deformation clearly show the fracturing of a cheese sample partly along a curd granule junction (Supplementary material Time-lapse video 3). This suggests the presence of localised weak zones along the curd granule junctions within the cheese matrix, which is probably due to the strength and types of bond formed between the networks of curd granules.

An inherent micro-defect (~32 µm; Fig. 7a) located at a curd granule junction was observed within the cheese matrix. During tensile deformation, the cheese sample not only fractured from the artificial notch but also fractured from the inherent defect located at this curd granule junction (Fig. 7b–e), and finally both cracks merged together (Fig. 7f) (Supplementary material Time-lapse video 4). Interestingly, the inherent defect fractured along the curd granule junction. This suggests that defect within the semi-hard cheese matrix is most likely to be present at the curd granule junction, in agreement with previous reports (Huc, Moulin, Mariette, & Michon, 2013; Huc et al., 2014). Moreover, defects at curd granule junctions tend to fracture along curd granule junction under deformation. This leads

us to hypothesise that the presence of micro-cracks within the cheese matrix could be precursors to splits and cracks observed in some eye-type cheeses; micro-cracks may grow gradually during ripening due to the stress exerted by the gas produced by micro-organisms, especially during warm-room ripening, when diffusion of gas at nuclei may create a tensile force within the cheese matrix.

Other studies have also observed micro-cracks (size ranging from 50 to 200 µm) in eye-type cheeses (Huc et al., 2013, 2014). The actual reasons for occurrence of inherent defects (micro-cracks) within the cheese matrix are not yet fully understood. However, entrapment of whey pockets, air bubbles or free fat between curd granules are considered as possible reasons, which may inhibit the formation of bonds between the network of curd granules (Akkerman, Walstra, & Van Dijk, 1989; Luyten & Van Vliet, 1996). It may also be possible that temperature variations between cheese curd granules during pressing and localised differences in composition and pH within the cheese matrix (Burdikova et al., 2015) could be contributory factors.

## 4. Conclusions

This study successfully achieved dynamic visualisation of semi-hard cheese microstructure under large-strain tensile deformation. On deformation, the fat globules/pools were detached from the protein network and subsequently released, confirming that the fat globules within semi-hard cheese matrix are not bonded to the protein matrix but rather weakly held/entrapped within the protein matrix. Moreover, the cheese matrix fractured (at least in part) along curd granule junctions, suggesting the presence of localised weak spots along the curd granule junctions within the cheese matrix. Inherent micro-defects were observed within the cheese matrix, and these defects are most likely to be present at the curd

granule junction. It is proposed that these micro-defects could be a key underlying factor in the formation of undesirable slits or cracks.

During fracturing, stress profiles of experimental cheeses varied with the levels of maturation, ripening temperature, coagulant type or residual chymosin activity, suggesting that the fracture behaviour of semi-hard cheese can be modulated by changing maturation levels, ripening temperature, using a different coagulant type, or inhibiting the residual chymosin activity. Overall, this study demonstrated the applicability of dynamic in situ imaging of cheese microstructure to better understand fat-protein interactions as well as predicting weak zones within a cheese matrix. Such structural information is particularly relevant for understanding sensory perception, as well as mechanisms of formation of undesirable slits and cracks within the cheese matrix. Furthermore, the approach used in this study could be applied to establish a greater understanding of structure-fracture relationships in cheese, as well as other food products.

## Acknowledgements

This study was funded by the Dairy Levy Trust Fund (RMIS 6259) administered by Dairy Research Ireland, and in part by Ornua (Dubin, Ireland). Prabin Lamichhane is currently in receipt of a Teagasc Walsh Fellowship. The authors acknowledge Prateek Sharma, Xiaofeng Xia, Vijaya Lakshmi Chirumamilla, and Ram Raj Panthi for technical assistance with cheese trials (all from Teagasc Food Research Centre, Moorepark, Fermoy, Co. Cork, Ireland).

## References

433 Abhyankar, A. R., Mulvihill, D. M., & Auty, M. A. E. (2011). Combined microscopic and
434 dynamic rheological methods for studying the structural breakdown properties of
435 whey protein gels and emulsion filled gels. *Food Hydrocolloids, 25*, 275–282.
436 Abhyankar, A. R., Mulvihill, D. M., & Auty, M. A. E. (2014). Combined confocal
437 microscopy and large deformation analysis of emulsion filled gels and stirred acid
438 milk gels. *Food Structure, 1*, 127–136.
439 Akkerman, J. C., Walstra, P., & Van Dijk, H. J. M. (1989). Holes in Dutch-type cheese. I:
440 Conditions allowing eye formation. *Netherlands Milk and Dairy Journal, 43*, 453–
441 476.
442 Alinovi, M., Cordioli, M., Francolino, S., Locci, F., Ghiglietti, R., Monti, L., et al. (2018).
443 Effect of fermentation-produced camel chymosin on quality of Crescenza cheese.
444 *International Dairy Journal, 84*, 72–78.
445 Auty, M. A. E., Fenelon, M. A., Guinee, T. P., Mullins, C., & Mulvihill, D. M. (1999).
446 Dynamic confocal scanning laser microscopy methods for studying milk protein
447 gelation and cheese melting. *Scanning, 21*, 299–304.
448 Bansal, N., Drake, M. A., Piraino, P., Broe, M. L., Harboe, M., Fox, P. F., et al. (2009).
449 Suitability of recombinant camel (*Camelus dromedarius*) chymosin as a coagulant for
450 Cheddar cheese. *International Dairy Journal, 19*, 510–517.
451 Barden, L. M., Osborne, J. A., McMahon, D. J., & Foegeding, E. A. (2015). Investigating the
452 filled gel model in Cheddar cheese through use of Sephadex beads. *Journal of Dairy*
453 *Science, 98*, 1502–1516.
454 Bast, R., Sharma, P., Easton, H. K. B., Dessev, T. T., Lad, M., & Munro, P. A. (2015).
455 Tensile testing to quantitate the anisotropy and strain hardening of mozzarella cheese.
456 *International Dairy Journal, 44*, 6–14.

Boitte, J. B., Hayert, M., & Michon, C. (2013). Observation of wheat flour doughs under mechanical treatment using confocal microscopy and classification of their microstructures. *Journal of Cereal Science, 58*, 365–371.

Brink, J., Langton, M., Stading, M., & Hermansson, A.-M. (2007). Simultaneous analysis of the structural and mechanical changes during large deformation of whey protein isolate/gelatin gels at the macro and micro levels. *Food Hydrocolloids, 21*, 409–419.

Burdikova, Z., Svindrych, Z., Pala, J., Hickey, C. D., Wilkinson, M. G., Panek, J., et al. (2015). Measurement of pH micro-heterogeneity in natural cheese matrices by fluorescence lifetime imaging. *Frontiers in Microbiology, 6*, Article 183.

Daly, D. F. M., McSweeney, P. L. H., & Sheehan, J. J. (2010). Split defect and secondary fermentation in Swiss-type cheeses – A review. *Dairy Science and Technology, 90*, 3–26.

El-Bakry, M., & Sheehan, J. (2014). Analysing cheese microstructure: A review of recent developments. *Journal of Food Engineering, 125*, 84–96.

Everett, D. W., & Auty, M. A. E. (2008). Cheese structure and current methods of analysis. *International Dairy Journal, 18*, 759–773.

Everett, D. W., & Auty, M. A. E. (2017). Cheese microstructure. In P. L. H. McSweeney, P. F. Fox, P. D. Cotter, & D. W. Everett (Eds.), *Cheese chemistry, physics and microbiology* (4th edn., pp. 547–569). San Diego, CA, USA: Academic Press.

Foegeding, E. A., Daubert, C. R., Drake, M. A., Essick, G., Trulsson, M., Vinyard, C. J., et al. (2011). A comprehensive approach to understanding textural properties of semi- and soft-solid foods. *Journal of Texture Studies, 42*, 103–129.

Geng, X. L., van den Berg, F. W. J., Bager, A. N., & Ipsen, R. (2011). Dynamic visualization and microstructure of syneresis of cheese curd during mechanical treatment. *International Dairy Journal, 21*, 711–717.

Granato, D., de Araújo Calado, V. M., & Jarvis, B. (2014). Observations on the use of statistical methods in food science and technology. *Food Research International, 55*, 137–149.

Guggisberg, D., Schuetz, P., Winkler, H., Amrein, R., Jakob, E., Fröhlich-Wyder, M.-T., et al. (2015). Mechanism and control of the eye formation in cheese. *International Dairy Journal, 47*, 118–127.

Huc, D., Mariette, F., Challois, S., Barreau, J., Moulin, G., & Michon, C. (2014). Multi-scale investigation of eyes in semi-hard cheese. *Innovative Food Science and Emerging Technologies, 24*, 106–112.

Huc, D., Moulin, G., Mariette, F., & Michon, C. (2013). Investigation of curd grains in Swiss-type cheese using light and confocal laser scanning microscopy. *International Dairy Journal, 33*, 10–15.

James, B., & Yang, S. W. (2011). Testing meat tenderness using an in situ straining stage with variable pressure scanning electron microscopy. *Procedia Food Science, 1*, 258–266.

Kappeler, S. R., van den Brink, H. M., Rahbek-Nielsen, H., Farah, Z., Puhan, Z., Hansen, E. B., et al. (2006). Characterization of recombinant camel chymosin reveals superior properties for the coagulation of bovine and camel milk. *Biochemical and Biophysical Research Communications, 342*, 647–654.

Lamichhane, P., Kelly, A. L., & Sheehan, J. J. (2018a). Symposium review: Structure-function relationships in cheese. *Journal of Dairy Science, 101*, 2692–2709.

Lamichhane, P., Kelly, A. L., & Sheehan, J. J. (2018b). Effect of milk centrifugation and incorporation of high-heat-treated centrifugate on the composition, texture, and ripening characteristics of Maasdam cheese. *Journal of Dairy Science, 101*, 5724–5737.

Lamichhane, P., Pietrzyk, A., Feehily, C., Cotter, P. D., Mannion, D. T., Kilcawley, K. N., et al. (2018c). Effect of milk centrifugation and incorporation of high heat-treated centrifugate on the microbial composition and levels of volatile organic compounds of Maasdam cheese. *Journal of Dairy Science, 101*, 5738–5750.

Lamichhane, P., Sharma, P., Kennedy, D., Kelly, A. L., & Sheehan, J. J. (2019). Microstructure and fracture properties of semi-hard cheese: Differentiating the effects of primary proteolysis and calcium solubilization. *Food Research International, 125*, 108525.

Le Tohic, C., O'Sullivan, J. J., Drapala, K. P., Chartrin, V., Chan, T., Morrison, A. P., et al. (2018). Effect of 3D printing on the structure and textural properties of processed cheese. *Journal of Food Engineering, 220*, 56–64.

Liu, K., Stieger, M., van der Linden, E., & van de Velde, F. (2015). Fat droplet characteristics affect rheological, tribological and sensory properties of food gels. *Food Hydrocolloids, 44*, 244–259.

Lopez, C. (2005). Focus on the supramolecular structure of milk fat in dairy products. *Reproduction Nutrition Development, 45*, 497–511.

Lopez, C., Camier, B., & Gassi, J.-Y. (2007). Development of the milk fat microstructure during the manufacture and ripening of Emmental cheese observed by confocal laser scanning microscopy. *International Dairy Journal, 17*, 235–247.

Luyten, H. (1988). *The rheological and fracture properties of Gouda cheese.* PhD thesis, Wageningen University, The Netherlands.

Luyten, H., & Van Vliet, T. (1996). Effect of maturation on large deformation and fracture properties of (semi-)hard cheeses *Netherlands Milk and Dairy Journal, 50*, 295–307.

McCarthy, C. M., Wilkinson, M. G., & Guinee, T. P. (2017). Effect of coagulant type and level on the properties of half-salt, half-fat Cheddar cheese made with or without

adjunct starter: Improving texture and functionality. *International Dairy Journal, 75*, 30–40.

McGoldrick, M., & Fox, P. F. (1999). Intervarietal comparison of proteolysis in commercial cheese. *Zeitschrift für Lebensmitteluntersuchung und -Forschung A, 208*, 90–99.

Moynihan, A. C., Govindasamy-Lucey, S., Jaeggi, J. J., Johnson, M. E., Lucey, J. A., & McSweeney, P. L. H. (2014). Effect of camel chymosin on the texture, functionality, and sensory properties of low-moisture, part-skim Mozzarella cheese. *Journal of Dairy Science, 97*, 85–96.

Öhgren, C., Langton, M., & Hermansson, A.-M. (2004). Structure-fracture measurements of particulate gels. *Journal of Materials Science, 39*, 6473-6482.

O'Mahony, J. A., Lucey, J. A., & McSweeney, P. L. H. (2005). Chymosin-mediated proteolysis, calcium solubilization, and texture development during the ripening of Cheddar cheese. *Journal of Dairy Science, 88*, 3101–3114.

Ong, L., Dagastine, R. R., Kentish, S. E., & Gras, S. L. (2011). Microstructure of milk gel and cheese curd observed using cryo scanning electron microscopy and confocal microscopy. *LWT-Food Science and Technology, 44*, 1291–1302.

Panthi, R. R., Kelly, A. L., Hennessy, D., O'Sullivan, M. G., Kilcawley, K. N., Mannion, D. T., et al. (2019). Effect of pasture versus indoor feeding regimes on the yield, composition, ripening and sensory characteristics of Maasdam cheese. *International Journal of Dairy Technology, 72*, 435–446.

Sala, G., van de Velde, F., Cohen Stuart, M. A., & van Aken, G. A. (2007). Oil droplet release from emulsion-filled gels in relation to sensory perception. *Food Hydrocolloids, 21*, 977–985.

Shakeel-Ur-Rehman, Feeney, E. P., McSweeney, P. L. H., & Fox, P. F. (1998). Inhibition of residual coagulant in cheese using pepstatin. *International Dairy Journal, 8*, 987–992.

Sharma, P., Munro, P. A., Dessev, T. T., Wiles, P. G., & Foegeding, E. A. (2018). Strain hardening and anisotropy in tensile fracture properties of sheared model Mozzarella cheeses. *Journal of Dairy Science, 101*, 123–134.

Somaratne, G., Nau, F., Ferrua, M. J., Singh, J., Ye, A., Dupont, D., et al. (2020). In-situ disintegration of egg white gels by pepsin and kinetics of nutrient release followed by time-lapse confocal microscopy. *Food Hydrocolloids, 98*, 105228.

Soodam, K., Ong, L., Powell, I. B., Kentish, S. E., & Gras, S. L. (2015). Effect of rennet on the composition, proteolysis and microstructure of reduced-fat Cheddar cheese during ripening. *Dairy Science and Technology, 95*, 665–686.

Soodam, K., Ong, L., Powell, I. B., Kentish, S. E., & Gras, S. L. (2017). Effect of elevated temperature on the microstructure of full fat Cheddar cheese during ripening. *Food Structure, 14*, 8–16.

Vandenberghe, E., Choucharina, S., De Ketelaere, B., De Baerdemaeker, J., & Claes, J. (2014). Spatial variability in fundamental material parameters of Gouda cheese. *Journal of Food Engineering, 131*, 50–57.

Visser, J. (1991). Factors affecting the rheological and fracture properties of hard and semi-hard cheese. *International Dairy Federation Bulletin, 268*, 49–61.

White, S. R., Broadbent, J. R., Oberg, C. J., & McMahon, D. J. (2003). Effect of *Lactobacillus helveticus* and *Propionibacterium freudenrichii* ssp. *shermanii* combinations on propensity for split defect in Swiss cheese. *Journal of Dairy Science, 86*, 719–727.

Zhang, Z., Jung, K.-J., Zhang, R., Muriel Mundo, J. L., & McClements, D. J. (2019). In situ monitoring of lipid droplet release from biopolymer microgels under simulated gastric conditions using magnetic resonance imaging and spectroscopy. *Food Research International, 123*, 181–188.

**Figure legends**

**Fig. 1.** Schematic of experimental set-up for microtensile testing, showing sample preparation and accessories related to microtensile testing.

**Fig. 2.** Effect of maturation on the fracture behaviour of control cheese: (a) representative profile of true stress and Hencky strain relationships (——, 20 d; – – -, 48 d; ----, 90 d); (b) box plots showing the Young's modulus of cheese samples as a function of maturation time; boxes not sharing common letters differ ($P < 0.05$), n = 2; (c) fracture stress and strain profile for cheese at (●) 20 d, (▼) 48 d and (■) 90 d of ripening; error bars represent standard errors of means, n = 2; (d) representative stress profile as a function of crack length; the black arrow in the graph indicates the starting point of fracture for cheese after (●) 20 d of ripening, while the grey arrow indicates the starting point of fracture for cheese after (▼) 48 d or (■) 90 d of ripening.

**Fig. 3.** Effect of treatment on fracture behaviour of semi-hard cheese at 48 d of ripening; experimental cheese variants were Control (control cheeses), noWR (cheeses without warm-room ripening), CC (cheeses made from fermentation-produced camel chymosin as a coagulant), and PepA (cheeses containing chymosin inhibitor, i.e., pepstatin A): (a) representative profile of true stress and Hencky strain relationships (——, Control; – – – , noWR; —— , CC; --- ---, PepA); (b) box plot showing the Young's modulus of experimental cheese variants; boxes not sharing common letters differ ($P < 0.05$), n = 2; (c) fracture stress and strain profile for (●) Control, (▼) noWR, (■) CC and (◆) PepA, error bars represent standard errors of means, n = 2; (d) representative stress profile as a function of crack length, the black arrow in the graph indicates the starting point of fracture for (▼)

noWR, (■) CC and (◆) PepA, whereas the grey arrow in the graph indicates the starting point of fracture for (●) Control.

**Fig. 4.** Selected confocal scanning laser microscopy (CSLM) micrographs of cheese obtained during tensile deformation of a notched sample, illustrating: (a) opening of the notch, (b–c) stretching of the protein network near the notch tip and (d–f) fracturing from notch tip. The arrow in micrograph (a) shows the artificial notch tip. Inset in micrograph (c) clearly shows the detachment of both small (5–7 µm) and large (15 µm) fat globules/pools from the protein network, suggesting that fat globules/pools are weakly held or entrapped within the semi-hard cheese matrix. The protein phase appears red while the fat phase appears green. Arrows beside the micrographs indicate the direction of tensile deformation.

**Fig. 5.** Selected confocal scanning laser microscopy micrographs of cheese (90 d of ripening) during tensile deformation of a notched sample, illustrating release of fat globules from the cheese matrix. The fat globule within the circle represents the same globule at different time points during tensile deformation. The protein phase appears red while the fat phase appears green. Arrows beside the micrographs indicate the direction of tensile deformation.

**Fig. 6.** Sequence of confocal scanning laser microscopy images of cheese obtained during tensile deformation of a notched cheese sample after 20 d of ripening, illustrating the growth of a crack partly along a curd granule junction. Long and short arrows show the crack tip and curd granule junction respectively. The protein phase appears red while the fat phase appears green. Arrows beside the micrographs indicate the direction of tensile deformation.

**Fig. 7.** Sequence of confocal scanning laser microscopy images of cheese taken during tensile deformation of a notched cheese sample after 90 d of ripening, illustrating the fracture behaviour in the presence of an inherent defect at a curd granule junction. The circle, in the micrograph and in the inset (a), shows the inherent defect (~32 µm) at a curd granule junction and the arrow shows the curd granule junction. Both the inherent defect and the notch (b–e) grew gradually and (f) merged during tensile deformation. The protein phase appears red while the fat phase appears green. Arrows beside the micrographs indicate the direction of tensile deformation.

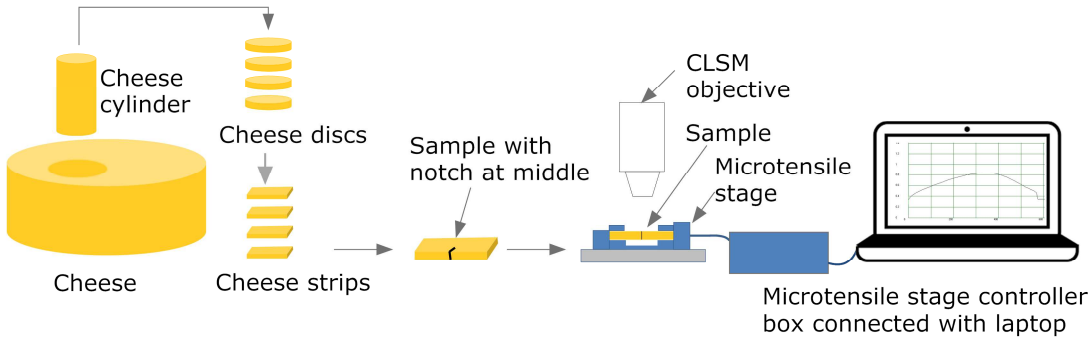




Fig. 1

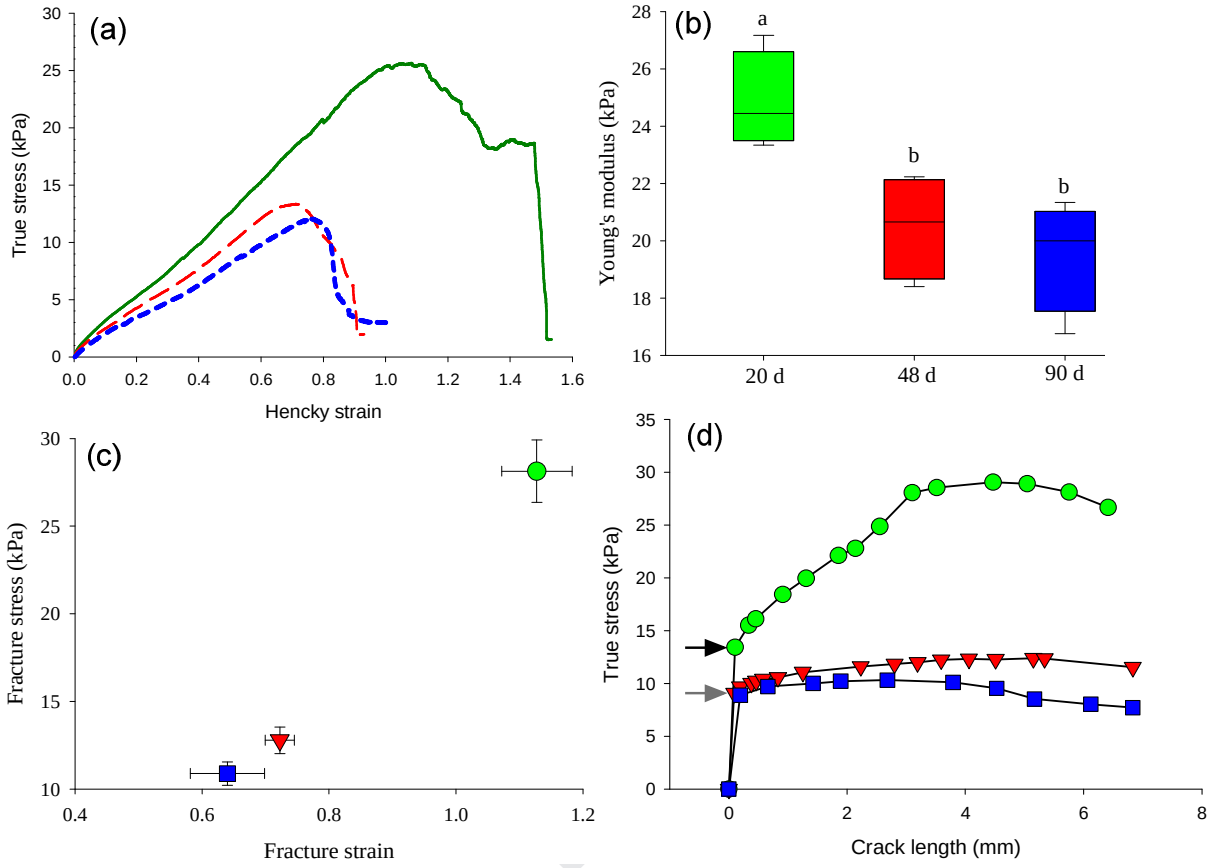


Fig. 2

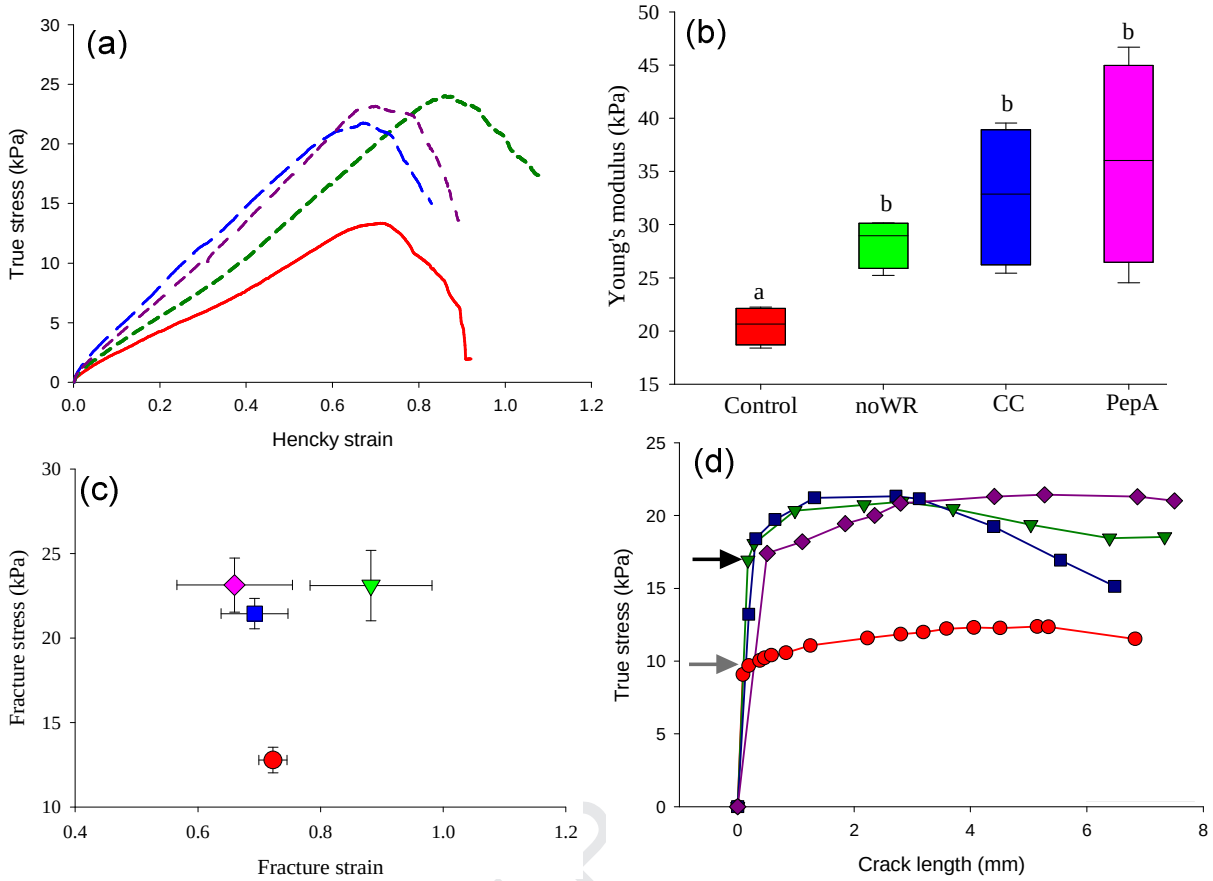




Fig. 3

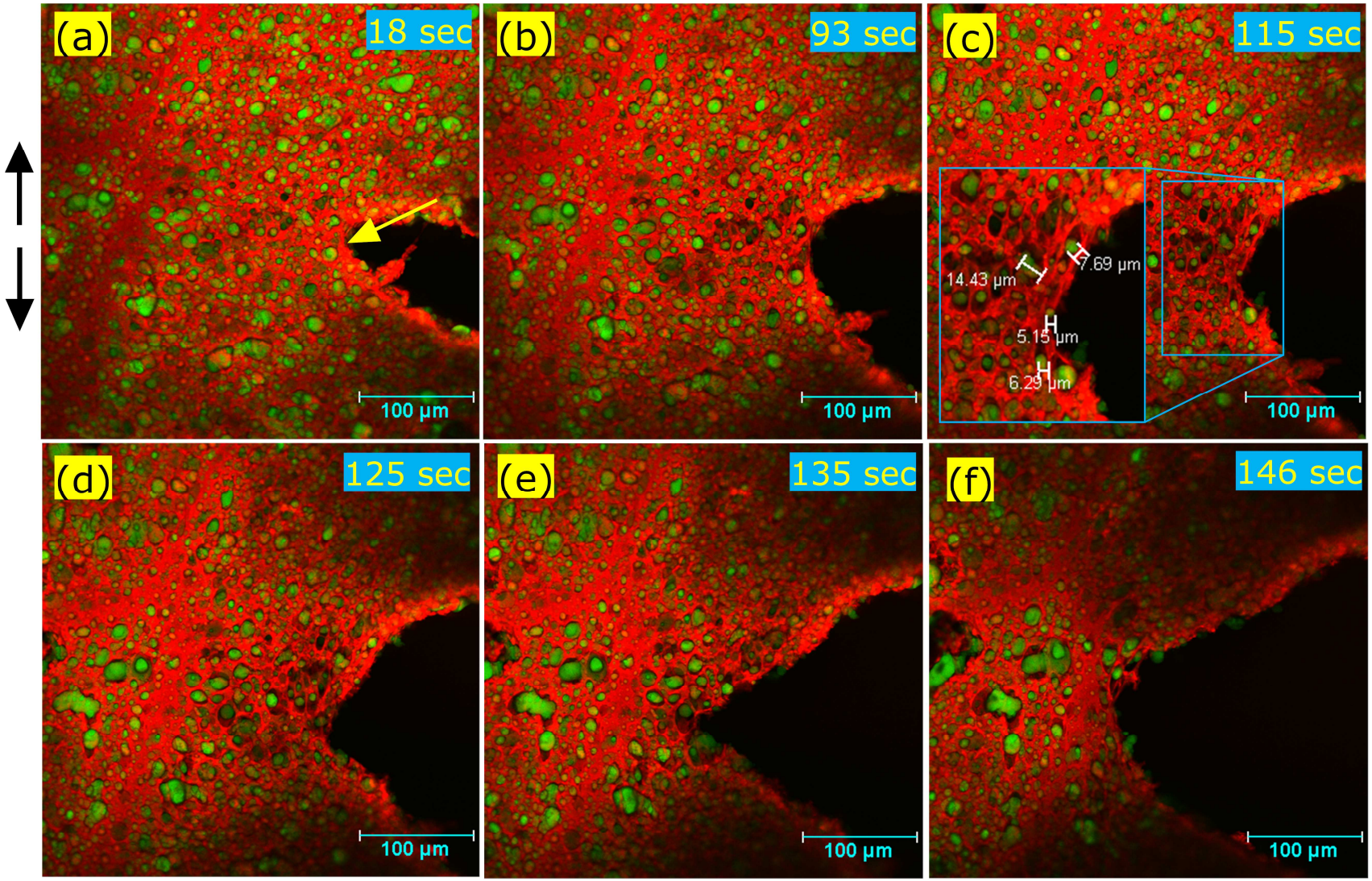
(a)
18 sec
100 µm
(b)
93 sec
100 µm
(c)
115 sec
14.43 µm
7.69 µm
5.15 µm
6.29 µm
100 µm
(d)
125 sec
100 µm
(e)
135 sec
100 µm
(f)
146 sec
100 µm

Fig. 4

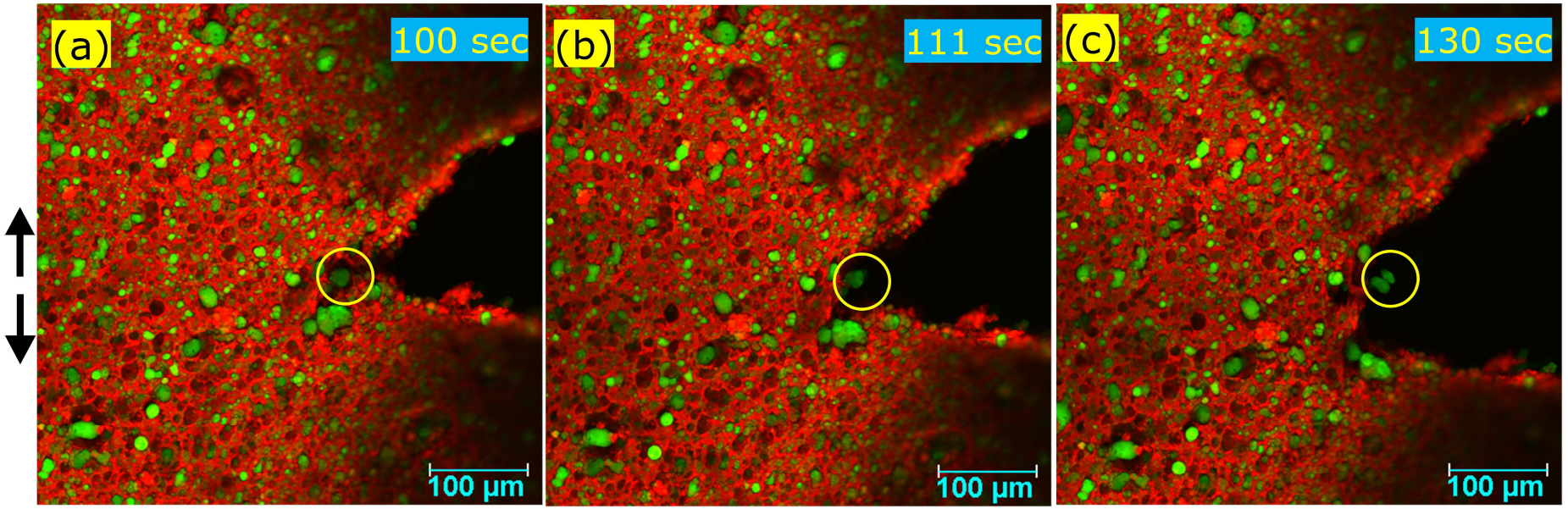




Fig. 5

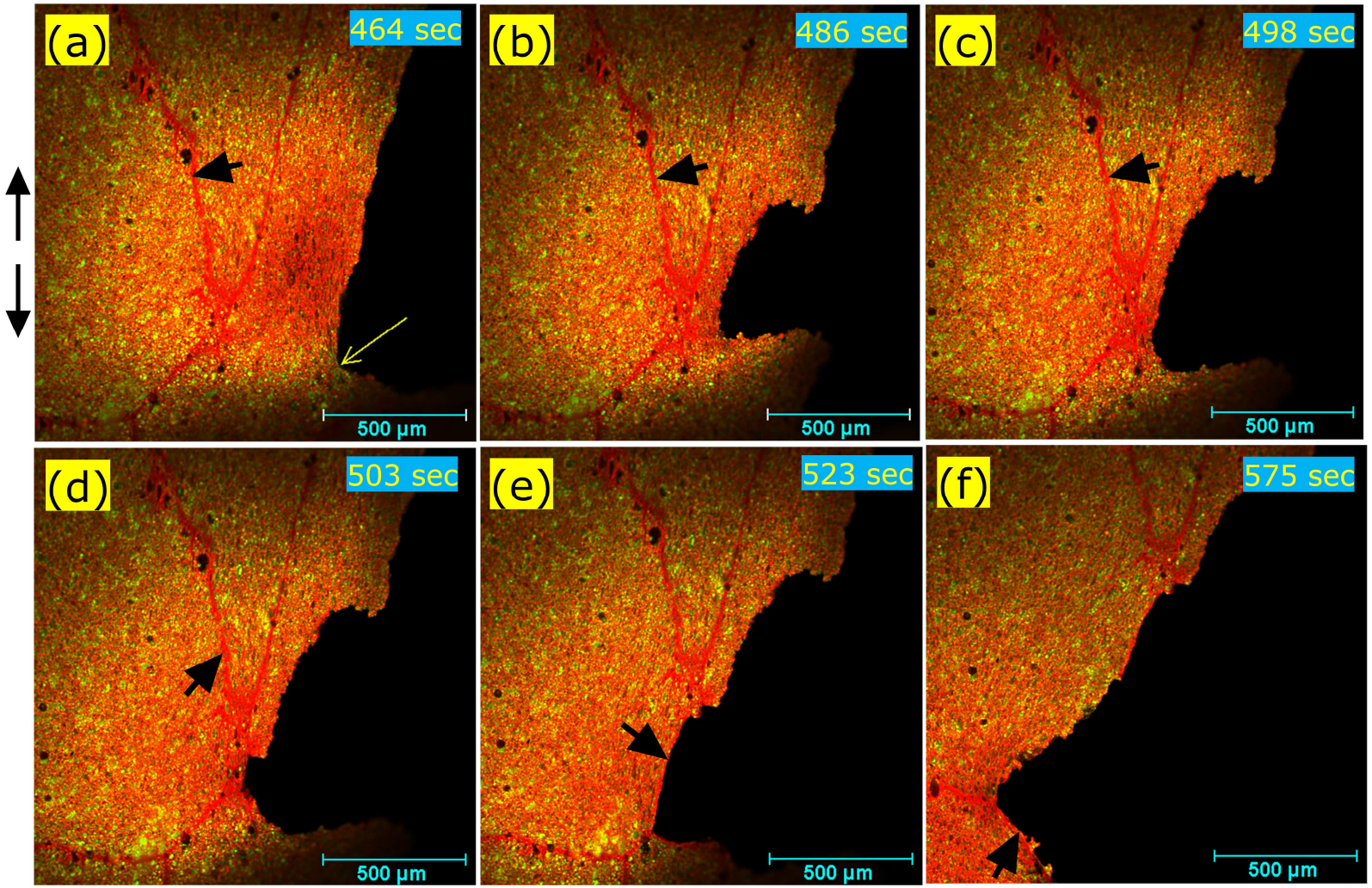
(a)
464 sec
500 µm
(b)
486 sec
500 µm
(c)
498 sec
500 µm
(d)
503 sec
500 µm
(e)
523 sec
500 µm
(f)
575 sec
500 µm

Fig. 6

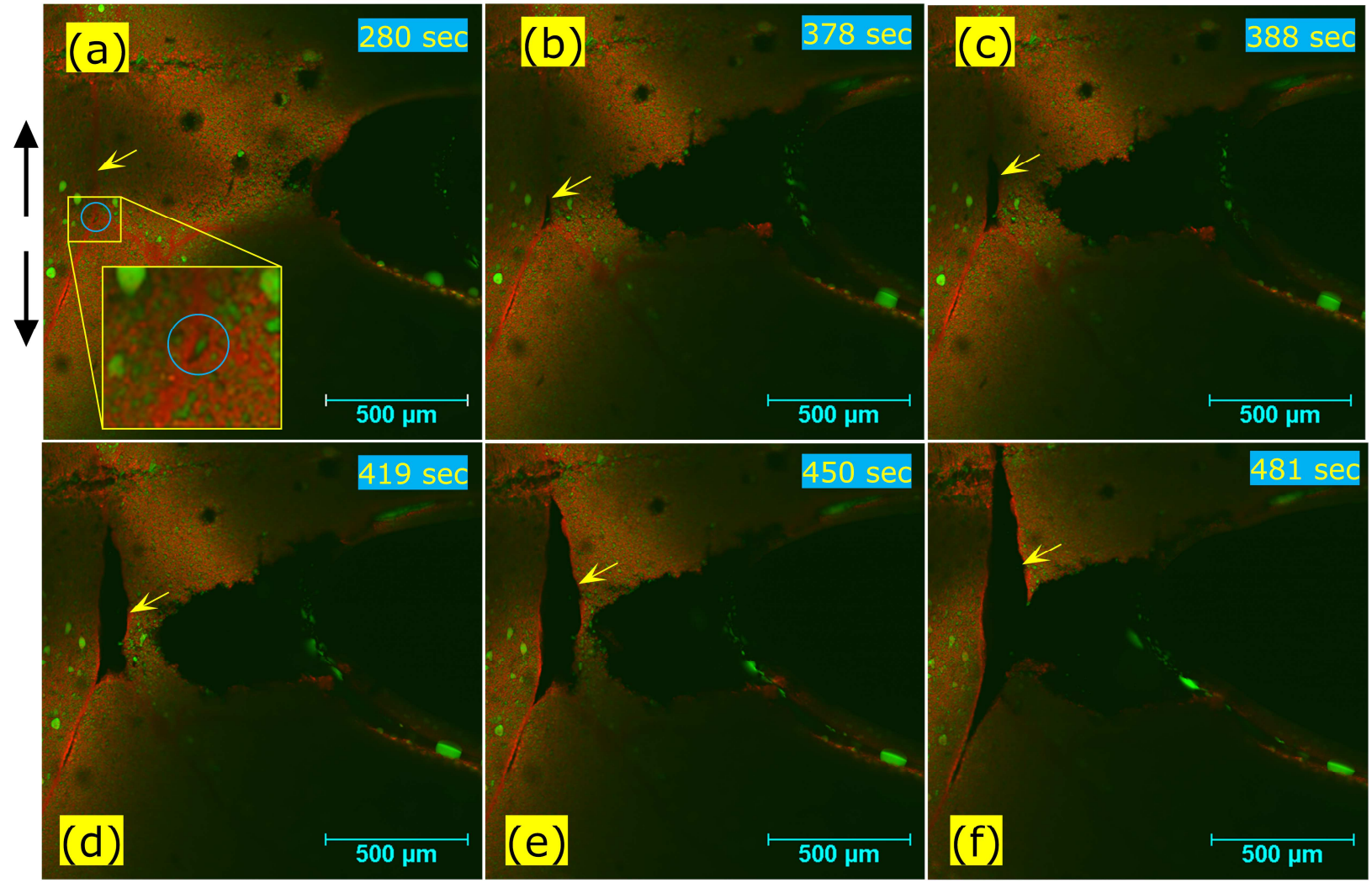
(a)
280 sec
500 µm
(b)
378 sec
500 µm
(c)
388 sec
500 µm
(d)
419 sec
500 µm
(e)
450 sec
500 µm
(f)
481 sec
500 µm

Fig. 7

**Author contributions:**

**Prabin Lamichhane:** Conceptualization, Methodology, Software, Formal analysis, Writing Original Draft, Visualization**.**

**Mark A.E. Auty:** Conceptualization, Methodology, Resources.

**Alan L Kelly:** Writing - Review & Editing, Supervision.

**Jeremiah J Sheehan:** Conceptualization, Resources, Writing - Review & Editing, Supervision, Funding acquisition.